Magnetic Exchange in $[Mn_2(\mu\text{-}O)_3(tmtacn)_2]^{2+}$: Metal−Metal Bonding or Superexchange?

Christopher D. Delfs and Robert Stranger*

Department of Chemistry, The Australian National University, Canberra ACT 0200, Australia

Received July 2, 1999

A computational study of the tris-μ-oxo-bridged manganese dimer $[Mn_2(\mu\text{-}O)_3(NH_3)_6]^{2+}$ as a model for $[Mn_2(\mu\text{-}O)_3(tmtacn)_2]^{2+}$ (tmtacn = N′,N″,N‴-trimethyl-1,4,7-triazacyclononane) has been undertaken to investigate the magnetic coupling in this complex. Although the complex has a very short Mn−Mn distance, 2.3 Å, and a large antiferromagnetic exchange constant, $2J_{ab} = -780$ cm^{-1}, the calculations reveal that the magnetic coupling is dominated by superexchange via the μ-oxo bridges and that direct Mn−Mn interaction is small.

Introduction

There has been an ongoing interest in the chemical and physical properties of oxomanganese clusters for several decades. The chemical synthesis, reactions, and physical properties of these systems are fascinating, not only from a purely academic viewpoint but also because they occur in a number of enzymes with various structures and functions such as manganese catalase and the oxygen evolving center of photosystem II.[1−4] Systems containing oxomanganese clusters are also of great interest in the synthesis of molecular magnetic compounds and have been used as starting materials to synthesize larger clusters with novel magnetic properties.[5,6]

Previously we have reported density functional calculations on the di-μ-oxo-bridged Mn dimers $[Mn_2(\mu\text{-}O)_2(NH_3)_8]^{n+}$ for $n = 2$, 3, and 4 and examined the nature of the exchange coupling in these complexes.[7,8] In general the $Mn^{IV}-Mn^{IV}$ distance is in the vicinity of 2.7 Å, and the magnetic coupling, which is dominated by superexchange via the bridges, corresponds to $2J_{ab} = -270$ cm^{-1}. In contrast the tri-μ-O-bridged species $[Mn_2(\mu\text{-}O)_3(tmtacn)_2]^{2+}$ exhibit very short Mn−Mn bond distances between 2.3 and 2.4 Å.[9−11] Given the very short Mn−Mn distances and the large magnetic exchange constant, $-2J_{ab} = 780$ cm^{-1}, the notion of direct overlap of metal orbitals is very appealing. However, by making comparisons of the structure of $[Mn_2(\mu\text{-}O)_3(tmtacn)_2]^{2+}$ with a number of related compounds, Wieghardt *et al.* could not make any definitive decision on whether metal−metal bonding was responsible for the large antiferromagnetic exchange. They concluded that $[Mn_2(\mu\text{-}O)_3(tmtacn)_2]^{2+}$ represented an "interesting borderline case".[9]

On the basis of the finding that, for confacial bioctahedra of first-row transition metals with a d^3-d^3 configuration, the magnetic exchange constant is related to the metal−metal separation by the expression

$$J_{ab} = 7.5 \times 10^6 \exp(-4R) \qquad (1)$$

Niemann *et al.*[11] concluded that direct overlap of the metal d_{z^2} orbitals was the sole pathway responsible for the magnetic exchange in this class of compounds. That is, superexchange through bridging ligands did not contribute to the magnetic exchange. The number of compounds for which eq 1 holds is surprisingly large, in that it is independent of both the bridging ligand and the transition metal ion. This in turn suggests that the magnetic behavior of this class of compounds is dominated by metal−metal bonding considerations.

An interesting comparison is the lack of any correlation between the copper−copper distance and the magnitude of the exchange constant in copper carboxylate dimers. The direct overlap of the $d_{x^2-y^2}-d_{x^2-y^2}$ orbitals (δ overlap) was one mechanism proposed to explain the magnetic properties of this series of compounds.[12] However, the absence of any r(Cu−Cu) to $-2J$ correlation was used to show that the magnetic coupling was dominated by a superexchange mechanism.[13]

Recently Zhao *et al.* investigated the bonding in a series of Mn dimers with μ-O and μ-RCO bridges and terminal tacn ligands.[14] Although they reported the results of a single-point calculation on $[Mn_2(\mu\text{-}O)_3(tacn)_2]^{2+}$, their analysis did not deal with the mechanism for the magnetic exchange in this compound. Accordingly, we intend to describe the results of our density functional calculations on the tri-μ-O-bridged species $[Mn_2(\mu\text{-}O)_3(tmtacn)_2]^{2+}$, using a model compound in which the tmtacn ligand is replaced by three ammonia molecules. Particular attention is paid to the magnetic exchange in this complex and

(1) Manchandra, R.; Brudvig, G.; Crabtree, R. H. *Coord. Chem. Rev.* **1995**, *144*, 1.
(2) Que, L., Jr.; True, A. E. *Prog Inorg. Chem.* **1990**, *38*, 97.
(3) Dismukes, G. C. *Chem. Rev.* **1996**, *96*, 2909−2926.
(4) Yachandra, V. K.; Sauer, K.; Klein, M. P. Chem. Rev. **1996**, *96*, 2927.
(5) Willett, R. D., Gatteschi, D., Kahn, O., Eds. *Magneto-structural correlations in exchange coupled systems*; NATO ASI series C; D. Riedel Publishing Co.: Dordrecht, The Netherlands, 1985; Vol. 140.
(6) Kahn, O. *Molecular Magnetism*; VCH Publishers: Weinheim, Germany, 1993.
(7) McGrady, J. E.; Stranger, R. *J. Am. Chem. Soc.* **1997**, *119*, 8512.
(8) Mcgrady, J. E.; Stranger, R. *Inorg. Chem.* **1999**, *38*, 550.
(9) Wieghardt, K.; Bossek, U.; Nuber, B.; Weiss, J.; Bonvoisin, J.; Corbella, M.; Vitols, S. E.; Girerd, J. J. *J. Am. Chem. Soc.* **1988**, *110*, 7398.
(10) Koek, J. H.; Russell, S. W.; van der Wolf, L.; Hage, R.; Warnaar, J. B.; Spek, A. L.; Kerschner, J.; Delpizzo, L. *J. Chem. Soc., Dalton Trans.* **1996**, 353.
(11) Niemann, A.; Bossek, U.; Wieghardt, K.; Butzlaff, C.; Trautwein, A. X. *Angew. Chem., Int. Ed. Engl.* **1992**, *31*, 311.
(12) Figgis, B. N.; Martin, R. L. *J. Chem. Soc.* **1956**, 3837.
(13) Goodgame, D. M. L.; Hill, N. J.; Marsham, D. F.; Skapski, A. C.; Smart, M. L.; Troughton, P. G. H. *J. Chem. Soc., Chem. Commun.* **1969**, 629.
(14) Zhao, X. G.; Richardson, W. H.; Li, J. L.; Noodleman, L.; Tsai, H. L.; Hendrickson, D. N. *Inorg. Chem.* **1997**, *36*, 1198.

10.1021/ic990790h CCC: $19.00
Published on Web 01/14/2000

how it relates to direct metal−metal overlap and superexchange mechanisms.

Computational Details

The calculations described in this work were performed on Linux/Pentium II based computers and Sun Ultra-SPARC 140/170 workstations using the density functional program ADF 2.3.0.[15,16] In addition to the exchange potential in the local density approximation, the correlation potential of Vosko, Wilk, and Nusair[17] and the Becke[18] and Perdew[19] corrections to the nonlocal exchange and correlation potentials were used. For the main group atoms N, O, and H, double-ζ basis functions with a single d polarization function were employed, and the 1s cores on the N and O were frozen. For the Mn atoms, triple-ζ functions were used with a 3p frozen core. Geometry optimizations were performed using the algorithm of Versluis and Zeigler.[20] D_{3h} symmetry was applied to calculations of the $S = 0$, 1, 2, and 3 spin states. Calculations using the broken-symmetry formalism were performed in C_{3v} symmetry.

Magnetic exchange constants ($H = -2JS_1 \cdot S_2$) were calculated using[21]

$$-2J = \frac{2(E(S_{max}) - E_B)}{S_{max}^2} \qquad (2)$$

where E_B is the energy of the broken symmetry state and $E(S_{max})$ is the energy of the highest possible spin state.

Results and Discussion

Orbital Interactions. We have previously described the bonding interactions in face-shared metal−halide bioctahedra for the d^3−d^3 configuration.[22−25] First appearances suggest that the qualitative features of the bonding should be the same in the isoelectronic complex $[Mn_2(\mu\text{-}O)_3(NH_3)_6]^{2+}$, namely, that a trigonal C_{3v} distortion to an essentially octahedral crystal field splits the formally metal t_{2g} orbitals into a_1 and e subsets while the e_g orbitals do not split but simply transform as another e representation. The occupied single ion a_1 and e orbitals, derived from the t_{2g} set, may participate in metal−metal σ and δ_π bonding, respectively,[26] as shown in Figure 1. In the weakly coupled (localized) limit, these orbitals remain essentially localized on the metals and are singly occupied, the ground-state singlet arising from antiparallel coupling of the spins on opposite centers. Metal−metal interaction, through either direct overlap of metal orbitals or superexchange, results in delocalization of the magnetic obitals over both metal centers and consequent formation of bonding $a_1'(\sigma)$, $e'(\delta_\pi)$ and antibonding $a_2''(\sigma^*)$, $e_2''(\delta_\pi^*)$ molecular orbitals based on D_{3h} symmetry of the dimer. The splittings within the energy levels shown in Figure 1 arise from two very different sources. In the weakly coupled limit spin polarization is responsible for the separation of the occupied and vacant single-ion orbitals, whereas in the delocalized limit the metal−metal interaction causes splitting between bonding and antibonding molecular orbitals. Thus, the

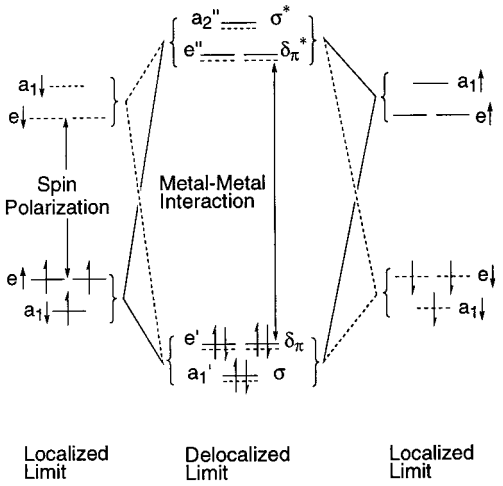

Figure 1. Representation of the broken-symmetry state of d^3−d^3 face-shared dimers in both the localized and delocalized limits.

delocalization of the magnetic electrons, and therefore the resulting geometry and extent of metal−metal interaction, will depend on the relative magnitudes of these two factors. Spin polarization favoring a localized description while metal−metal interaction, by either direct metal orbital overlap or superexchange, results in delocalization.

Without making any assumptions regarding the extent of delocalization of the metal-based orbitals, the broken-symmetry state can always be defined in C_{3v} symmetry by the antiferromagnetic configuration $(a_1\uparrow)^1(a_1\downarrow)^1(e\uparrow)^2(e\downarrow)^2(e\uparrow)^0(e\downarrow)^0(a_1\uparrow)^0(a_1\downarrow)^0$, where the magnetic electrons on adjacent centers have opposite spin. The extent to which the magnetic orbitals involved in the broken-symmetry state are delocalized over both metal centers can be determined from the composition of the relevant molecular orbitals.

There are three spin states, $S = 3$, 2, and 0, normally associated with the broken-symmetry state of d^3−d^3 confacial bioctahedra. Each of these spin states is represented by a single configuration, corresponding to a different level of metal−metal interaction, and are defined here using the full molecular symmetry (D_{3h}). The $S = 3$ associated state has the configuration $(6a_1'\uparrow)^1(8e'\uparrow)^2(6e''\uparrow)^2(5a_2''\uparrow)^1$; that is, it contains the same number of bonding and antibonding electrons and consequently corresponds to a bond order of zero. The $S = 2$ associated state, $(6a_1'\uparrow)^1(6a_1'\downarrow)^1(8e'\uparrow)^2(6e''\uparrow)^2$, has a bond order of one, a σ bond and no net δ_π bonding. Finally, the $S = 0$ associated state $(6a_1'\uparrow)^1(6a_1'\downarrow)^1(8e'\uparrow)^2(8e'\downarrow)^2$, corresponds to a triple bond; that is, the σ and δ_π orbitals are fully occupied and the σ^* and δ_π^* orbitals are vacant. For the series of metal−halide dimers, the metal−metal separations at which the minima for the pure spin states occur were found to be largely insensitive to the metal ion, with bond distances of approximately 2.4, 2.9, and 3.3 Å corresponding to the $S = 0$, $S = 2$, and $S = 3$ associated states, respectively.[22−25]

In terms of the Heisenberg Hamiltonian, the $S = 3$ associated state arises from the coupling of two $S = 3/2$ ions and as such is part of a set of spin states $S = 0$, 1, 2, 3. To avoid confusion, we will refer to such a set of states as a spin ladder. In the $S = 2$ associated state described above, two electrons are involved in a formal σ bond, leaving two unpaired δ_π electrons on each Mn ion. Therefore, in terms of the Heisenberg Hamiltonian, this state is a member of the spin ladder arising from the coupling of two $S = 1$ ions. Finally the $S = 0$ state has no unpaired electrons. The broken-symmetry state is a mixture of all the $M_S = 0$ states within one spin ladder, and the connection

(15) Baerends, E. J.; Ellis, D. E.; Ros, P. *Chem. Phys.* **1973**, *2*, 41.
(16) te Velde, G.; Baerends, E. J. *J. Comput. Phys.* **1992**, *99*, 84.
(17) Vosko, S. H.; Wilk, L.; Nusair, M. *Can. J. Phys.* **1980**, *58*, 1200.
(18) Becke, A. D. *Phys. Rev. A* **1988**, *38*, 3098.
(19) Perdew, J. P.; Chevary, J. A.; Vosko, S. H.; Jackson, K. A.; Pederson, M. R.; Singh, D. J.; Fiolhais, C. *Phys. Rev. B* **1992**, *46*, 6671.
(20) Versluis, L.; Ziegler, T. J. *J. Chem. Phys.* **1988**, 322.
(21) Noodleman, L. J. *Chem. Phys.* **1981**, *74*, 5737.
(22) McGrady, J. E.; Lovell, T.; Stranger, R. *Inorg. Chem.* **1997**, *36*, 3242.
(23) McGrady, J. E.; Stranger, R.; Lovell, T. *J. Phys. Chem.* **1997**, *101*, 6265.
(24) Lovell, T. Electronic structure and bonding in face shared and edge shared transition metal dimer complexes. Ph.D. Thesis, The Australian National University, 1998.
(25) McGrady, J. E.; Stranger, R.; Lovell, T. *Inorg. Chem.* **1998**, *37*, 3802.
(26) Trogler, W. *Inorg. Chem.* **1980**, *19*, 697.

Table 1. Experimental and Calculated Geometry Parameters, Relative Bond Energies, and Spin Density for the $[Mn_2(\mu\text{-}O)_3(NH_3)_6]^{2+}$ Cation

	$S=0$	$S=1$	$S=2$	$S=3$	BS	obsd
Mn−Mn	1.904	2.413	2.147	2.416	2.320	2.30−2.41
Mn−O	1.878	1.818	1.846	1.862	1.840	1.82−1.86
Mn−N	2.157	2.181	2.174	2.181	2.184	2.09−2.17
Mn−O−Mn	60.9	83.03	71.11	80.97	78.10	78−80
bond energy	0.00	−2.6407	−3.5650	−3.6414	−4.1614	
spin density						
Mn_1			1.92	2.92	2.54	
Mn_2			1.92	2.92	−2.54	

between the broken-symmetry state and the associated full-symmetry states $S = 0$, 2, and 3 can be described as follows. When the magnetic coupling is weak, the highest and lowest spin states within that spin ladder must lie close in energy. For example, when the broken-symmetry and $S = 3$ states are close, the two Mn ions are weakly coupled. Similarly, when the broken-symmetry state and $S = 2$ states are close, then the four δ_π electrons are weakly coupled and the remaining two σ electrons are strongly coupled, that is, involved in bonding interactions. Finally, when the Mn−Mn separation is small enough to form a σ and two δ_π bonds, the $S = 0$ state is the ground state. In this case, there is only one $M_S = 0$ level, and as such, the broken-symmetry and $S = 0$ states converge.

In principle, it is also possible to define an $S = 1$ associated state with the configuration $(6a_1'\uparrow)^1(8e'\uparrow)^2(8e'\downarrow)^2(5a_2''\uparrow)^1$, corresponding to a δ_π double bond but with no net σ bonding. Considering only the metal−metal interactions, it is difficult to imagine how such a state could be the ground state or contribute to the bonding in these compounds. Only with the inclusion of large contributions from ligand-based orbitals is it possible for this $S = 1$ state to impact the bonding in this class of compounds. This point is discussed later in more detail.

Geometry Optimizations. The results of geometry optimizations for the broken-symmetry state and each of the associated spin states are given in Table 1. The calculated parameters for the broken-symmetry state fall in the experimentally observed range of values, with the exception of the Mn−N distance, which is slightly longer than crystallographically determined values. A separate calculation optimizing the geometry of the broken-symmetry state of $[Mn_2(\mu\text{-}O)_3(tacn)_2]^{2+}$ found that the structure of the central core is the same as in $[Mn_2(\mu\text{-}O)_3(NH_3)_6]^{2+}$. However, a shorter Mn−N distance was calculated at 1.994 Å, which presumably can be attributed to the macrocyclic effect. Of interest is that the calculated Mn−Mn bond distance in $[Mn_2(\mu\text{-}O)_3(NH_3)_6]^{2+}$ increases from 1.904 to 2.147 to 2.416 Å for the $S = 0$, $S = 2$, and $S = 3$ states, respectively, which is the result of the decrease in formal bond order from three to zero. However, relative to other d^3−d^3 dimers, these distances are all very short. For example, in a series of calculations on isoelectronic $[Mn_2F_9]^-$, we found that the minima for the $S = 0$, $S = 2$, and $S = 3$ states occur at 2.28, 2.54, and 2.78 Å, respectively.[27] Yet in $[Mn_2(\mu\text{-}O)_3(NH_3)_6]^{2+}$, the $S = 3$ state, with its calculated r(Mn−Mn) of 2.416 Å, corresponds to *no* metal−metal bonding. Therefore, the short Mn−Mn distances, of 2.3−2.4 Å observed experimentally, must be the result of other interactions. The obvious candidates are the bonding interactions between the metals and the bridging μ-O ligands.

Magnetic Exchange. Using eq 2 and the bond energies given in Table 1, the magnetic exchange constant is calculated to be $-2J = 932$ cm^{-1} with $S_{max} = 3$, in good agreement with the experimental value of 780 cm^{-1}. With $S_{max} = 2$ the calculated magnetic exchange constant is much larger, $-2J = 2405$ cm^{-1}, and therefore significant Mn−Mn σ bonding is unlikely to be present. Zhao *et al.* reported a value of $-2J = 1378$ cm^{-1} from single-point calculations, using experimental geometries idealized to C_s symmetry and $S_{max} = 3$.[14] The difference between the exchange constant calculated by Zhao *et al.* and that obtained in the present study can be largely attributed to the fact that we have used optimized geometries for both the broken-symmetry and $S = 3$ states. However, this agreement can be considered somewhat fortuitous in the sense that eq 2 is strictly only valid when the chosen S_{max} and broken-symmetry states are close in energy.[23] As will be discussed later, the optimized broken-symmetry state with r(Mn−Mn) = 2.320 Å does not lie close in energy to any of the pure spin states described above.

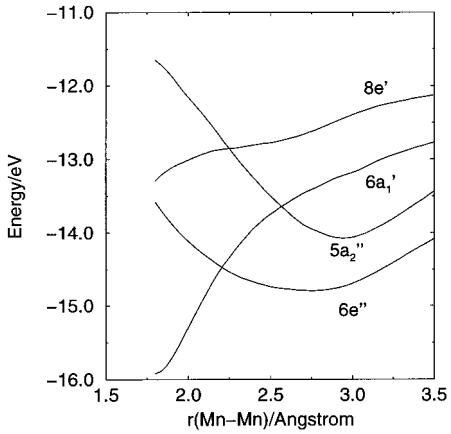

Figure 2. Energy levels of the spin-up magnetic orbitals from the $S = 3$ state plotted as a function of the Mn−Mn separation for $[Mn_2(\mu\text{-}O)_3(NH_3)_6]^{2+}$.

The magnetic exchange interactions and metal−metal bonding can be broken down into separate contributions according to the irreducible representations of the point group symmetry. In $[Mn_2(\mu\text{-}O)_3(NH_3)_6]^{2+}$ there are only two pathways to consider. The first is the interaction between σ (d_{z^2}) orbitals on the two metal centers which belongs to the a_1 representation. The second, which is the result of interaction between the δ_π orbitals on the two metal centers, belongs to the e representation. Since both pathways, a_1 and e, can be the result of metal−metal bonding or superexchange, any distinction between them must be based on the extent to which ligand orbitals contribute to the relevant magnetic orbitals.

The variation in energy of the magnetic orbitals from the $S = 3$ spin-unrestricted calculations are plotted in Figure 2. The energy difference between the symmetric and asymmetric combinations of a pair of orbitals in the S_{max} state is known to reflect the magnitude of the antiferromagnetic component of a particular exchange pathway[6,28−30]. In a system where bridging ligands make little or no contribution to these orbitals, the general expectation is that at long distances the σ and σ* levels will be close in energy, similarly for the δ_π and δ_π* orbitals. However, this figure shows that at 3.5 Å metal−metal separation, the δ_π* orbital 6e″ is 1.96 eV lower than the δ_π orbital 8e′. The obvious candidate for this discrepancy is that at least one of these orbitals contains large contributions from the

(27) Delfs, C. D.; Stranger, R. Unpublished data.

(28) Hay, P. J.; Thibeault, J. C.; Hoffmann, R. *J. Am. Chem. Soc.* **1975**, *97*, 4884.
(29) Brown, C. A.; Remar, G. J.; Musselmann, R. L.; Solomon, E. I. *Inorg. Chem.* **1995**, *34*, 688.
(30) Barone, V.; Bencini, A.; Ciofini, I.; Daul, C.; Totti, F. *J. Am. Chem. Soc.* **1998**, *120*, 8357.

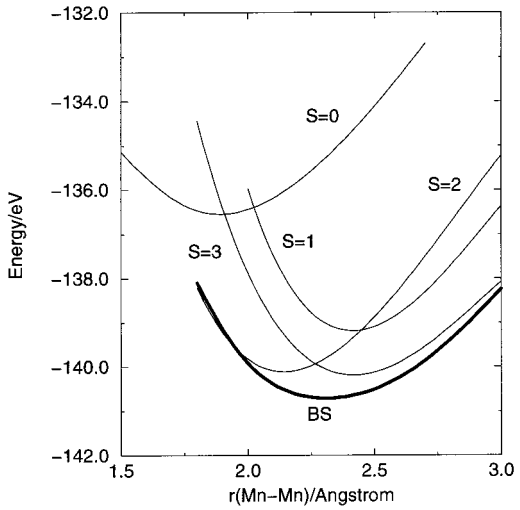

Figure 3. Potential energy curves for the $S = 0$, $S = 1$, $S = 2$, $S = 3$, and broken-symmetry states in $[Mn_2(\mu\text{-}O)_3(NH_3)_6]^{2+}$.

Table 2. Composition of the Spin-Up Molecular Orbitals Derived From a Mulliken Population Analysis of the Broken-Symmetry State Calculated at a Mn−Mn Separation of 2.320 Å

	Mn1	Mn2	O
$10a_1$	46.93	6.49	41.41
13e	43.77	14.62	35.28
14e	10.39	65.72	20.40
$11a_1$	6.17	76.98	14.28

bridging ligands. Analysis of the atomic orbital contributions to 8e′ shows it is 2/3 metal based and 1/3 bridging ligand. In contrast 6e″ is almost entirely metal based. This is because the orientation of the relevant O p orbitals is such that overlap with the δ_π orbitals of the metal is small. In the broken-symmetry state the symmetry requirements are relaxed, allowing substantial interaction between the metal d_{xz} and d_{yz} orbitals and the bridging ligand p orbitals. In comparison with the σ and σ^* molecular orbitals, the energy difference between 8e′(δ_π) and 6e″(δ_π^*) is relatively constant over the range of metal−metal distances from 2.3 to 3.5 Å. It is not until the metal separation drops below 1.8 Å that the 6e″ orbital is energetically higher than 8e′. The σ and σ^* orbitals show a similar inversion at long Mn−Mn separations. Only at approximately 2.5 Å does the $6a_1'$ orbital fall below $5a_2''$, indicating that direct d_{z^2}-d_{z^2} overlap is now more important than superexchange via the μ-O bridges for this magnetic exchange pathway. At the experimental Mn−Mn distance, 2.3 Å, the separation between the 6e″ and 8e′ orbitals is approximately twice the separation between the $6a_1'$ and $5a_2''$ orbitals, suggesting the δ_π pathway is the major contributor to the magnetic exchange.

Broken-Symmetry Analysis. Table 2 shows the contribution of the two Mn^{4+} ions and the bridging O^{2-} anions to the $\sigma(\uparrow)$, $\sigma^*(\uparrow)$, $\delta_\pi^*(\uparrow)$, and $\delta^\pi(\uparrow)$ molecular orbitals ($10a_1$, $11a_1$, 13e, and 14e, respectively) obtained from broken-symmetry calculations. The composition of the corresponding down-spin orbitals, which are degenerate with the up-spin orbitals, can be obtained from the latter by swapping the Mn1 and Mn2 contributions. There are two obvious points to be made from these data. First, the small contributions from Mn2 to the $10a_1$ orbital shows that this molecular orbital is, to a large extent, localized on one metal center, indicating direct Mn−Mn σ bonding is small. Second, the occupied $10a_1$ and 13e magnetic orbitals have large contributions from the bridging O^{2-} as was suggested by the analysis of the spin-unrestricted $S = 3$ calculations. This implies

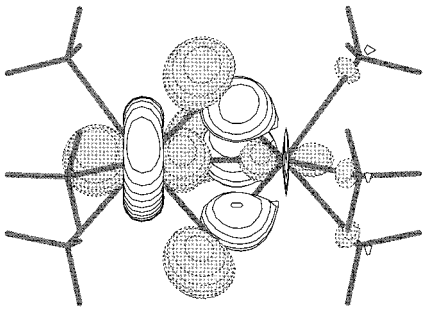

Figure 4. A pseudo-three-dimensional plot of the $10a_1$ orbital in $[Mn_2(\mu\text{-}O)_3(NH_3)_6]^{2+}$. The cutoff contour is 0.05 $(e/Å^3)^{1/2}$.

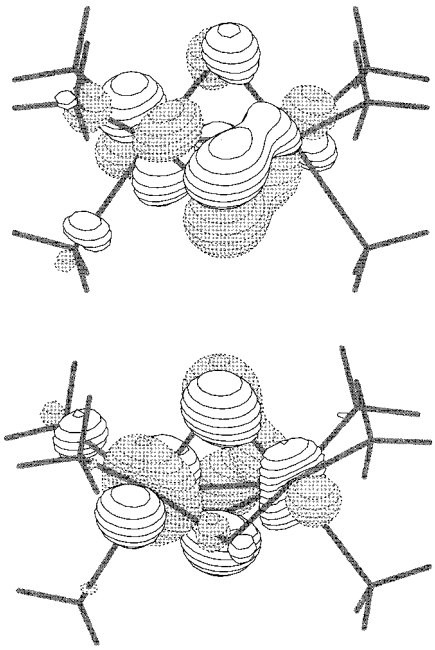

Figure 5. A pseudo-three-dimensional plot the 13e orbitals in $[Mn_2(\mu\text{-}O)_3(NH_3)_6]^{2+}$. The cutoff contour is 0.05 $(e/Å^3)^{1/2}$.

that superexchange mechanisms, mediated by the bridging O^{2-}, make significant contributions to the overall magnetic exchange. A third point that can be made about these results is that the delocalization in the 13e(δ_π^*) orbital is approximately 2.5 times greater than that in $10a_1(\sigma)$, suggesting this is the principal exchange pathway. The $10a_1$ and 13e orbitals are shown in Figures 4 and 5, respectively. Figure 4 shows that direct d_{z^2}-d_{z^2} overlap cannot be ignored but is nevertheless small. Conversely Figure 5 shows substantial overlap between the ligand p and metal δ_π orbitals.

To further investigate the metal−metal interaction in $[Mn_2(\mu\text{-}O)_3(NH_3)_6]^{2+}$, we have calculated the energies of the broken-symmetry and $S = 0$, 1, 2, and 3 associated states as a function of the Mn−Mn separation. The resulting potential energy curves are shown in Figure 3. This figure clearly shows that the broken-symmetry state, at the experimental metal separation, is not well approximated by any of the pure spin states. The $S = 3$ curve has a minimum at 2.416 Å, and at this distance the broken-symmetry curve is substantially lower in energy. Similarly the $S = 2$ curve does not converge with the broken-symmetry curve until r(Mn− Mn) is less than 2.0 Å. That is, the broken-symmetry state, at r(Mn−Mn) = 2.3 Å, is not well approximated by a state with the spins fully localized on the Mn ions nor by a state with metal−metal σ bonding. However, at this distance the curve for the $S = 3$ state lies closer to the broken-symmetry curve than $S = 2$ and therefore

represents the best S_{max} state to use in eq 2. Also shown is the curve of the $S = 1$ state with the configuration $(6a_1'\uparrow)^1(6e''\uparrow)^2(6e''\downarrow)^2(5a_2''\uparrow)^1$. This is the lowest energy triplet and represents the state which would converge with the broken-symmetry state if the σ electrons were localized but the δ_π electrons were completely delocalized via superexchange involving the 2p orbitals on the bridging O^{2-} ligands.

It is useful to compare the magnetic exchange interaction in $[Mn_2(\mu\text{-}O)_3(NH_3)_6]^{2+}$ with a related compound, $[Fe_2(\mu\text{-}OH)_3(tmtacn)_2]^{2+}$.[29] This compound is considered a rare example of a class III mixed valence Fe(II)−Fe(III) dimer. In a series of density functional computations on this compound, Barone *et al.* calculated the separate contributions of the magnetic exchange and double exchange terms to the $S = 9/2$ spin ladder.[30] As is the case in the present study, the superexchange in the iron dimer was found to be predominantly via the e pathway, involving the δ_π metal orbitals and bridging ligand p orbitals. In contrast to the manganese dimer, the σ and σ^* orbitals of the mixed valence iron dimer have very small contributions from the bridging ligands and exhibit significant $d_{z^2}-d_{z^2}$ overlap and hence delocalization of the *odd* electron in the σ^* orbital. Accordingly, it seems reasonable to attribute the lack of $d_{z^2}-d_{z^2}$ overlap in $[Mn_2(\mu\text{-}O)_3(NH_3)_6]^{2+}$ to the contraction of the 3d orbitals in the formally Mn^{4+} compared to Fe^{3+} and Fe^{2+}. The contracted nature on these orbitals would normally lead to increased single-ion spin polarization energy and thus, on the basis of Figure 1, a more localized description of the magnetic orbitals.[22,23,31] However, we have previously shown that the increased metal−ligand covalency arising from the higher charge on Mn^{4+} compared to M^{3+} ions actually results in a smaller spin polarization term for Mn^{4+} than Cr^{3+}. Thus, it can be concluded that the decrease in the metal orbital overlap largely contributes to the localization of the metal-based σ electrons in $[Mn_2(\mu\text{-}O)_3(NH_3)_6]^{2+}$. The more or less localized description of the σ electrons is consistent with the calculated spin density of 2.54 on the Mn centers, given in Table 1. The departure from the value of 2.92 calculated for the $S = 3$ state can be largely attributed to partial delocalization of the δ_π electrons as a result of superexchange.

(31) Charles W. Bauschlicher, J.; Walch, S. P.; Langhoff, S. R. In *Qunatum Chemistry: The challenge of transition metals and coordination chemistry*; Veillard, A., Ed.; D. Reidel: Dordrecht, The Netherlands, 1985; Vol. 176.

Conclusions

The results of our calculations have shown that the large antiferromagnetic exchange observed in tris-μ-O-bridged manganese dimers consists of a complicated mixture of direct and superexchange pathways. The notion of direct overlap of the d_{z^2} orbitals to form a metal−metal σ bond is appealing because of the very short Mn−Mn distance observed in these compounds. However, we have found that all possible exchange pathways involve significant contributions from the μ-O bridging ligands. Although we cannot entirely rule out direct metal orbital overlap as a contributor to the total magnetic exchange interaction, the results of these calculations show that the unpaired spin density is largely localized for the $10a_1$ magnetic orbital, which is the pathway responsible for metal−metal σ bonding. The magnetic orbitals were found to be approximately 40% O^{2-} 2p character, and the delocalization of the spin density in the 13e orbitals was approximately 2.5 times that in the $10a_1$ orbital. Hence, it is concluded that the dominant magnetic exchange pathway is superexchange via the δ_π orbitals on the metal ions and the 2p orbitals on the μ-O bridges. These results are contrary to the perfectly reasonable conclusions made by Niemann *et al.* based on the experimentally determined magnetic exchange constants and metal−metal separations of a range of confacial bioctahedra of first-row transition metal complexes. We can only postulate that the reason $[Mn_2(\mu\text{-}O)_3(NH_3)_6]^{2+}$ fits neatly into this magnetostructural correlation is that the superexchange contribution to the magnetic exchange is comparable to that expected for direct overlap of the metal d_{z^2} orbitals.

Acknowledgment. The Australian Research Council is gratefully acknowledged for financial support.

IC990790H